

# Microwave-Assisted Synthesis of C/SiO<sub>2</sub> Composite with Controllable Silica Nanoparticle Size

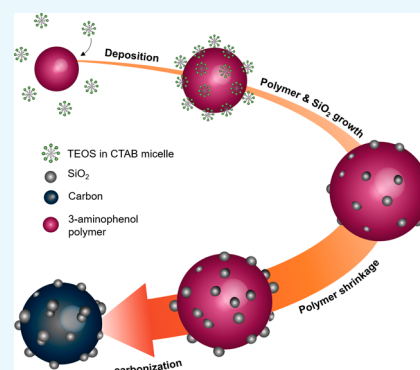
Aditya F. Arif,<sup>†</sup> Shuto Taniguchi,<sup>†</sup> Takafumi Izawa,<sup>†,‡</sup> Kazuki Kamikubo,<sup>†</sup> Hideharu Iwasaki,<sup>‡</sup> and Takashi Ogi<sup>\*,†</sup>

<sup>†</sup>Department of Chemical Engineering, Graduate School of Engineering, Hiroshima University, 1-4-1 Kagamiyama, Higashi-hiroshima, Hiroshima 739-8527, Japan

<sup>‡</sup>Battery Materials Research Laboratory, Kurashiki Research Center, Kuraray Co., Ltd., 2045-1 Sakazu, Kurashiki, Okayama 710-0801, Japan

## S Supporting Information

**ABSTRACT:** A C/SiO<sub>2</sub> composite was produced from 3-aminophenol and tetraethyl orthosilicate (TEOS) by a synthesis protocol that involved microwave irradiation. This protocol featured simultaneous 3-aminophenol polymerization and TEOS hydrolysis and condensation, which were achieved rapidly in a microwave reactor. The SiO<sub>2</sub> component was formed from low-concentration TEOS confined in cetyltrimethylammonium bromide micelles. We demonstrated a control of the SiO<sub>2</sub> particle size, ranging from 20 to 90 nm, by varying the 3-aminophenol concentration. The carbon component provided a microporous structure that greatly contributed to the high specific surface area, 375 m<sup>2</sup>/g, and served as a host for the nitrogen functional groups with a content of 5.34%, 74% of which were pyridinic type. The composite formation mechanism was clarified from time-series scanning electron microscopy images and dynamic light scattering analysis. An understanding of the composite formation mechanism in this protocol will enable the design of composite morphologies for specific applications.



## 1. INTRODUCTION

The unique characteristics of carbon, such as high mechanical strength,<sup>1</sup> high electrical conductivity,<sup>2</sup> tunable properties,<sup>3</sup> and its low cost, have led to its extensive use in many fields. The widespread applications of carbon have attracted in-depth studies of this material with the aim of functional improvements. One area of interest is structural modification, which encompasses the morphology and chemical structure. Work aimed at engineering the morphological structure has established synthesis protocols for various carbon structures, e.g., dense, porous, hollow, and fibrous.<sup>3–6</sup> Methods for modification of the chemical structure range from the atomic scale, e.g., heteroatom doping, to the macro scale, e.g., composite formation. Composites of carbon with other materials such as metals or metal oxides are particularly attractive because of the growing demand for high-performance devices that need to combine the features of more than one material.

SiO<sub>2</sub> is a common constituent of carbon composites. SiO<sub>2</sub> is used in many products because of its natural abundance, thermal stability, and dielectric properties.<sup>7,8</sup> Previous research on the synthesis of C/SiO<sub>2</sub> composites has led to improved electrical properties, microwave absorption, metal immobilization, and resistance to organic solvents.<sup>9–14</sup> There are three possible approaches to the synthesis of general carbon/silicon oxide composites. The first involves mechanical mixing of presynthesized materials such as silicon oxide nanoparticles and

graphite.<sup>15,16</sup> In the second approach, a presynthesized material such as SiO<sub>2</sub> nanoparticles is combined with a raw material such as sucrose as the carbon source.<sup>17</sup> Although composite synthesis using presynthesized materials is generally simple, control of the constituent morphology and characteristics is easier when the raw materials for both constituents are used as the starting materials; this is the third possible approach. The challenge is to develop a simple, rapid method for composite synthesis that gives good control of the composite structure.

For C/SiO<sub>2</sub> composite formation, the Stöber method can be used to synthesize SiO<sub>2</sub> from alkoxysilanes such as tetraethyl orthosilicate (TEOS). A method based on the same principle is also effective for the synthesis of carbon from 3-aminophenol.<sup>18,19</sup> Recently, our group improved this method by using microwave irradiation to accelerate polymerization of carbon source monomers, namely 3-aminophenol and hexa-(methoxymethyl)melamine, to give nitrogen-doped hollow carbon spheres.<sup>20,21</sup>

In the present study, we used a combination of SiO<sub>2</sub> production from TEOS by the Stöber method and carbon production from 3-aminophenol to synthesize a C/SiO<sub>2</sub> composite with a controllable SiO<sub>2</sub> particle size. The synthesis protocol features rapid 3-aminophenol polymerization simulta-

**Received:** February 25, 2018

**Accepted:** April 4, 2018

**Published:** April 11, 2018

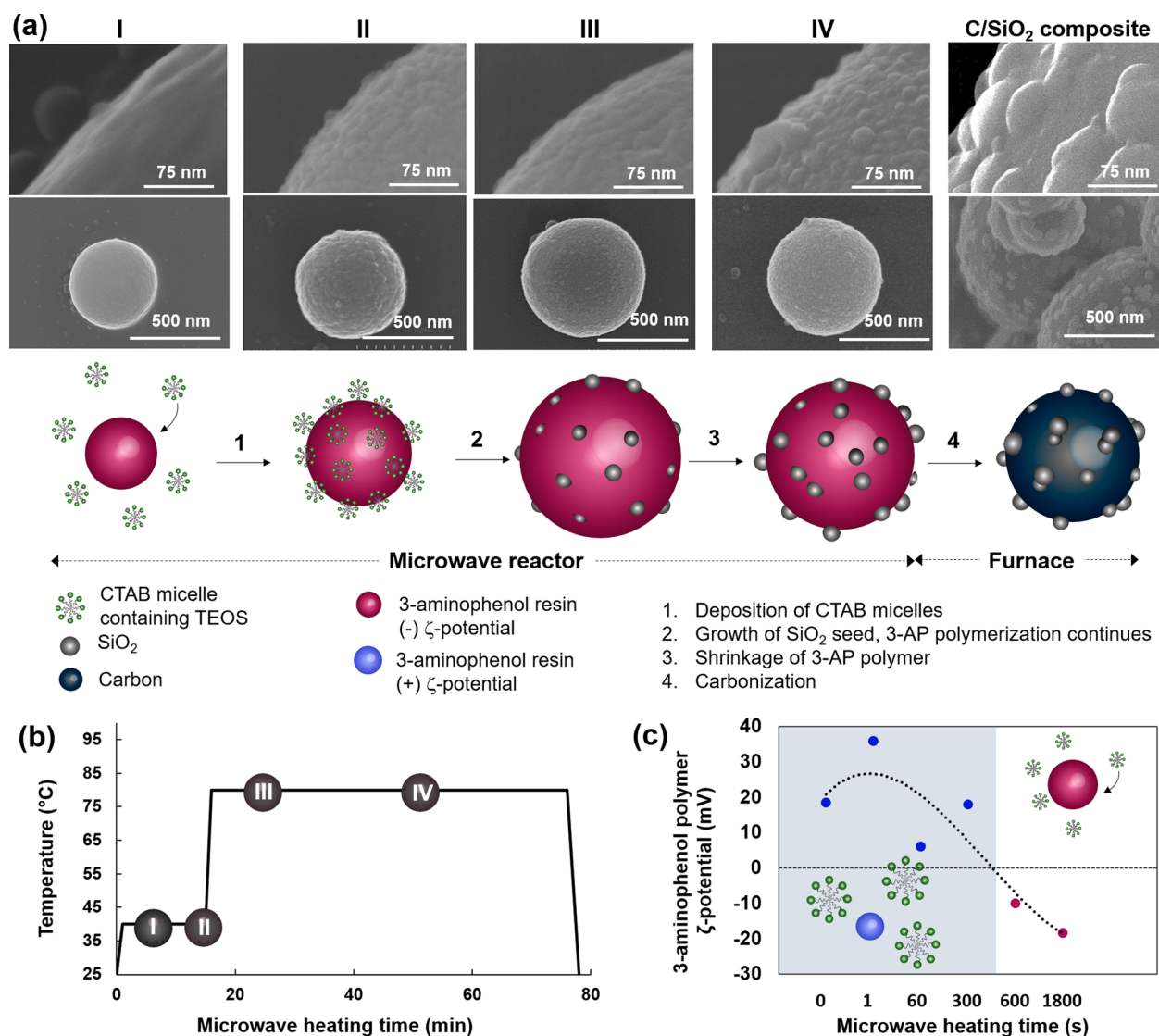


**Figure 1.** (a) Composite formation mechanism explained by changes in particle morphology after microwave irradiation at 40 °C for 7 min (step I) and 15 min (step II), at 80 °C for 10 min (step III) and 30 min (step IV), and after carbonization; (b) microwave heating pattern, showing times at which samples were taken; and (c) changes in  $\zeta$ -potential during 3-aminophenol polymerization.

neously with hydrolysis-condensation of TEOS under microwave irradiation. The controllable SiO<sub>2</sub> particle size enables more flexible design of the carbon/SiO<sub>2</sub> interface area, which is a critical consideration in some applications. We also used time-series images of the morphological structure and dynamic light scattering (DLS) to investigate the composite formation mechanism in this synthesis protocol. An understanding of the composite formation mechanism will enable future improvements in composite morphology design.

## 2. RESULTS AND DISCUSSION

**2.1. Composite Formation Mechanism.** In this protocol, the carbon and SiO<sub>2</sub> components were synthesized simultaneously in a microwave reactor. Observation of the changes in the particle morphology under microwave irradiation therefore provided an effective approach to clarifying the composite formation mechanism. Scanning electron microscopy (SEM) images of the particle samples during microwave irradiation were therefore obtained. Figure 1a shows the images for

samples taken at four different times, following the pattern described in Figure 1b.

3-Aminophenol was considered to be homogeneously nucleated before entering the reactor, as in our previous study.<sup>22</sup> Simultaneously, cetyltrimethylammonium bromide (CTAB) micelles were formed, with the hydrophobic tail attracted to ethanol. Formaldehyde and TEOS were introduced into the solution at the same time. Polymerization of 3-aminophenol was initiated immediately after the addition of formaldehyde, and TEOS was stabilized inside the CTAB micelles. Hydrolysis of TEOS was slower than 3-aminophenol polymerization; therefore, TEOS was unreacted when 3-aminophenol polymerization started. Figure 1c shows that the  $\zeta$ -potential of the 3-aminophenol polymer changed with microwave irradiation time. The  $\zeta$ -potential of the polymer was positive at the beginning of polymerization because the dominant charge came from the amine group;<sup>22</sup> the CTAB micelle  $\zeta$ -potential (25 mV) was also positive because CTAB is a cationic surfactant. As a consequence of having identical charges, the 3-aminophenol polymer and CTAB micelles were

independent before microwave irradiation, as shown in the inset in Figure 1c.

Composite formation under microwave irradiation was divided into four stages, according to sampling time. The first sample was taken after microwave irradiation for 7 min at 40 °C. Figure 1c shows that the  $\zeta$ -potential of the 3-aminophenol polymer changed to negative after irradiation for approximately 6 min and therefore had a charge opposite to that of the CTAB micelles. The change in the  $\zeta$ -potential was stimulated by the formation of OH<sup>-</sup> groups on the polymer surface.<sup>22</sup> Consequently, the CTAB micelles were electrostatically attracted to the 3-aminophenol polymer and were deposited on its surface. This is confirmed by the presence of trace SiO<sub>2</sub> seeds on the surface of the 3-aminophenol polymer in the SEM image of the first stage in Figure 1a. The presence of SiO<sub>2</sub> seeds also indicates that TEOS hydrolysis had already started.

The growth of SiO<sub>2</sub> nanoparticles continued as microwave irradiation was sustained. In the second stage, the particle surfaces became rough as more SiO<sub>2</sub> seeds were attached and grew on the polymer surface. In the third stage, the heating temperature was increased to 80 °C, which resulted in higher rates of TEOS hydrolysis and condensation. However, the polymerization of 3-aminophenol continued concurrently with the growth of SiO<sub>2</sub>. The growing 3-aminophenol polymer concealed the SiO<sub>2</sub> nanoparticles. The composite surface was therefore smoother in the third stage than in the second stage, as seen in Figure 1a.

Our previous research<sup>22</sup> showed that the size of the 3-aminophenol polymer increased to a certain maximum value before shrinking in the final stage of polymerization. Shrinkage of the 3-aminophenol polymer is the reason for the surfacing of SiO<sub>2</sub> nanoparticles after microwave irradiation for 30 min at 80 °C, as seen in the SEM images for stage IV.

Carbonization caused further shrinkage and the composite particle size decreased from 1025 to 715 nm. It was the carbon constituent that shrank. The heat applied during carbonization and the decrease in the carbon volume caused SiO<sub>2</sub> agglomeration after carbonization, as shown in Figure 1a. The final SiO<sub>2</sub> particle size was approximately 65 nm.

Another relevant point is that the SiO<sub>2</sub> nanoparticles were much smaller than the CTAB micelles. DLS measurements showed that the average CTAB micelle size was approximately 120 nm. A supporting experiment involving neither 3-aminophenol nor formaldehyde gave SiO<sub>2</sub> particles of size close to that of the micelles. This suggests that the SiO<sub>2</sub> particles and micelles were of similar size. The smaller SiO<sub>2</sub> particle size in the composite can be ascribed to electrostatic interactions between CTAB micelles and the 3-aminophenol polymer. As mentioned earlier, the  $\zeta$ -potential of the 3-aminophenol polymer changed with polymerization time because of changes in the dominant functional group. The inconsistent  $\zeta$ -potential disturbed the electrostatic system in the solution, and this affected the micelle stability. The disturbed electrostatic system induced the formation of smaller aggregates on the polymer surface.<sup>23</sup>

An important point is that CTAB played a critical role in composite formation in this synthesis protocol. We performed an in-depth study of this issue by observing the effect of the CTAB concentration on composite formation, as shown in Figure 2. In the absence of CTAB, no SiO<sub>2</sub> was observed on the carbon particles, as shown in Figure 2a. CTAB is a cationic surfactant and is therefore positively charged, which facilitates attraction to the negatively charged polymer. However, no free

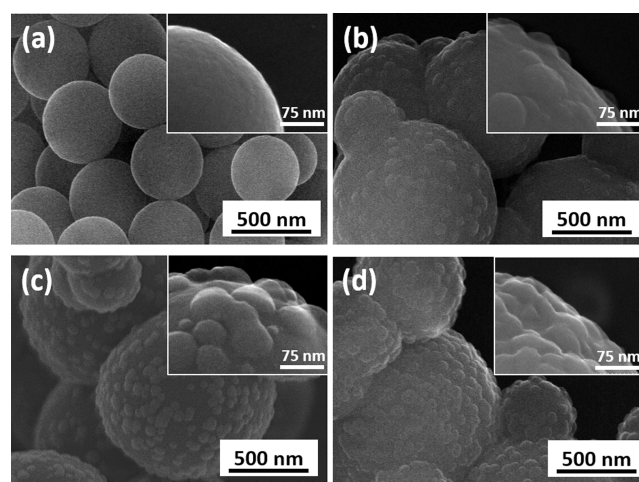


**Figure 2.** Morphologies of particles synthesized with addition of (a) 0 g, (b) 0.25 g, (c) 0.5 g, and (d) 1 g of CTAB.

SiO<sub>2</sub> particles were found in the absence of CTAB. On the basis of this finding, an additional experiment was conducted in which SiO<sub>2</sub> particles were prepared by the Stöber method but with microwave irradiation instead of conventional heating. The concentration of TEOS used in this additional experiment was the same as that used in the synthesis of the SiO<sub>2</sub>/C composite. Unlike the case in previous research, no SiO<sub>2</sub> particles were obtained from this experimental protocol, probably because of the low TEOS concentration (Figure S1).<sup>24</sup> However, SiO<sub>2</sub> was successfully synthesized when CTAB was added to the system. These results imply that CTAB not only assisted the deposition of SiO<sub>2</sub> nanoparticles on the surface of the 3-aminophenol polymer but also facilitated SiO<sub>2</sub> formation by concentrating TEOS in the micelles.

Figure 2b shows traces of SiO<sub>2</sub> nanoparticles on the surface of the 3-aminophenol polymer when a small amount (0.25 g) of CTAB was added to the composite precursor. Increasing the CTAB concentration resulted in the presence of more SiO<sub>2</sub> on the particle surface, as shown in the insets in Figure 2c,d, but the numbers of SiO<sub>2</sub> particles in Figure 2c,d are comparable. This is a reasonable trend because the number of micelles in the precursor solution generally increased with increasing CTAB concentration. However, the micellar properties of CTAB in the ethanol–water system tend to be constant at high CTAB concentrations.<sup>25</sup>

**2.2. Control of SiO<sub>2</sub> Nanoparticle Size and Composite Characteristics.** In this study, the stability of the CTAB micelles was altered by changes in the electrostatic system caused by formation of a 3-aminophenol polymer. In line with this finding, DLS measurements showed that the CTAB micelle size decreased with increasing amount of 3-aminophenol added, indicating an affinity of CTAB micelles for 3-aminophenol (Figure S2). This phenomenon, which is the result of interactions between the CTAB micelles and the 3-aminophenol monomer and polymer, was used to tailor the SiO<sub>2</sub> nanoparticle size.

Figure 3 shows the morphologies of composites synthesized with various 3-aminophenol concentrations before and after carbonization. The amount of CTAB used was 0.5 g. A summary of the composite and SiO<sub>2</sub> particle sizes as a function of 3-aminophenol concentration is provided in Figure 4a. Increasing the 3-aminophenol concentration resulted in larger composite particles because of the increased fraction of the

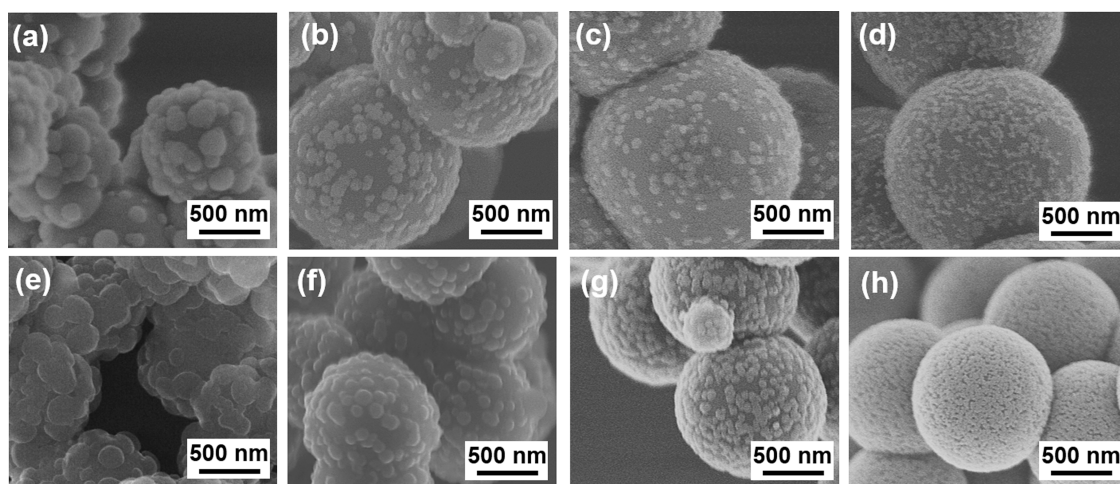


**Figure 3.** SEM images of 3-aminophenol polymer/SiO<sub>2</sub> composites (a–d) and C/SiO<sub>2</sub> composites (e–h) synthesized with different 3-aminophenol concentrations: 12 μM (a, e), 24 μM (b, f), 36 μM (c, g), and 48 μM (d, h).

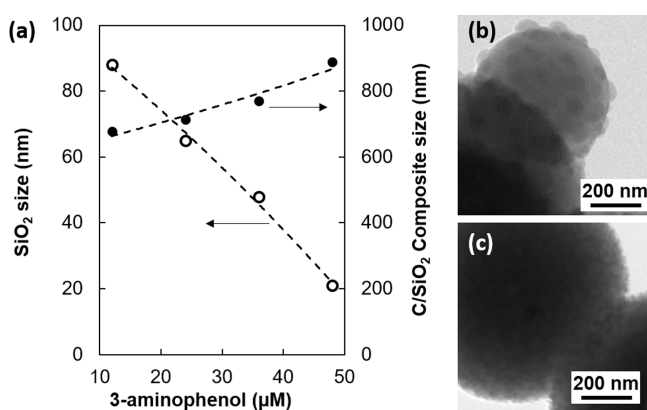


**Figure 4.** (a) Effect of 3-aminophenol concentration on SiO<sub>2</sub> and composite particle size, and transmission electron microscopy (TEM) images of C/SiO<sub>2</sub> composite synthesized using 3-aminophenol concentrations of (b) 24 μM and (c) 48 μM.

carbon constituent. This result is in accordance with those of our previous research on the synthesis of hollow carbon particles from 3-aminophenol.<sup>22</sup> The results also show that the SiO<sub>2</sub> nanoparticle size decreased with increasing 3-aminophenol concentration. DLS measurements of the 3-aminophenol polymer ζ-potential showed that the ζ-potential is independent of 3-aminophenol concentration.<sup>18</sup> This suggests that the ζ-potential could disrupt the micellar morphology by breaking it into smaller aggregates but does not determine the final SiO<sub>2</sub> particle size. Previous studies showed that the micellar shape and size can be changed by increasing the ionic activity, e.g., by salt addition.<sup>26</sup> The same phenomenon could occur in the 3-aminophenol system, triggering changes in the SiO<sub>2</sub> particle size when the amount of 3-aminophenol is changed. In addition, the size of the 3-aminophenol polymer increased with increasing 3-aminophenol concentration. This results in a larger available surface for SiO<sub>2</sub> seed deposition and promotes homogeneous deposition and better SiO<sub>2</sub> dispersion.

The TEM images in Figure 4b,c show apparent dispersion of SiO<sub>2</sub> nanoparticles. However, it is difficult to distinguish SiO<sub>2</sub>

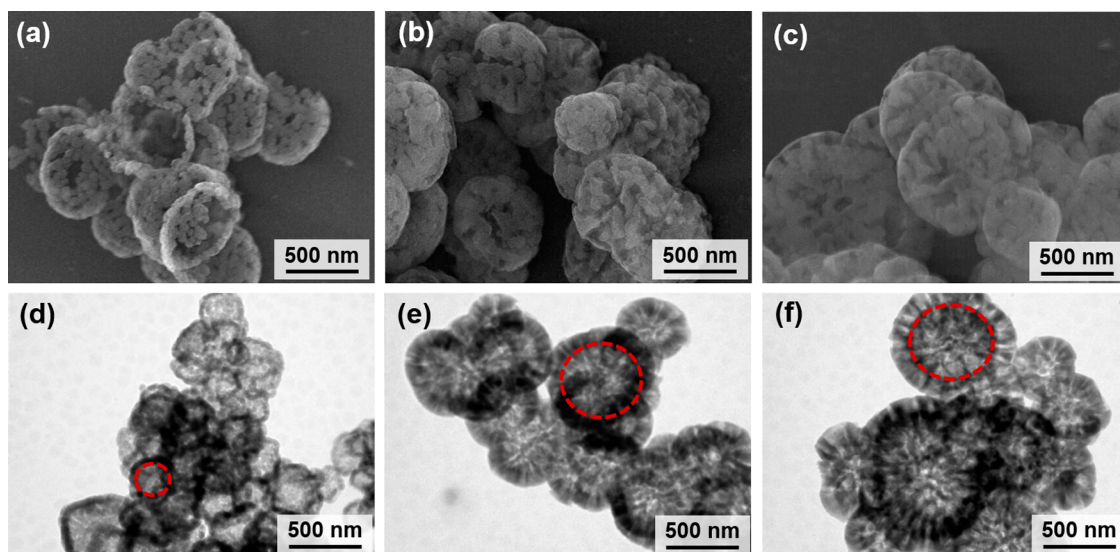


**Figure 5.** SEM (a–c) and TEM (d–f) images after calcination of composites with 3-aminophenol/TEOS ratios of (a, d) 1:0.25, (b, e) 1:0.5, and (c, f) 1:1.

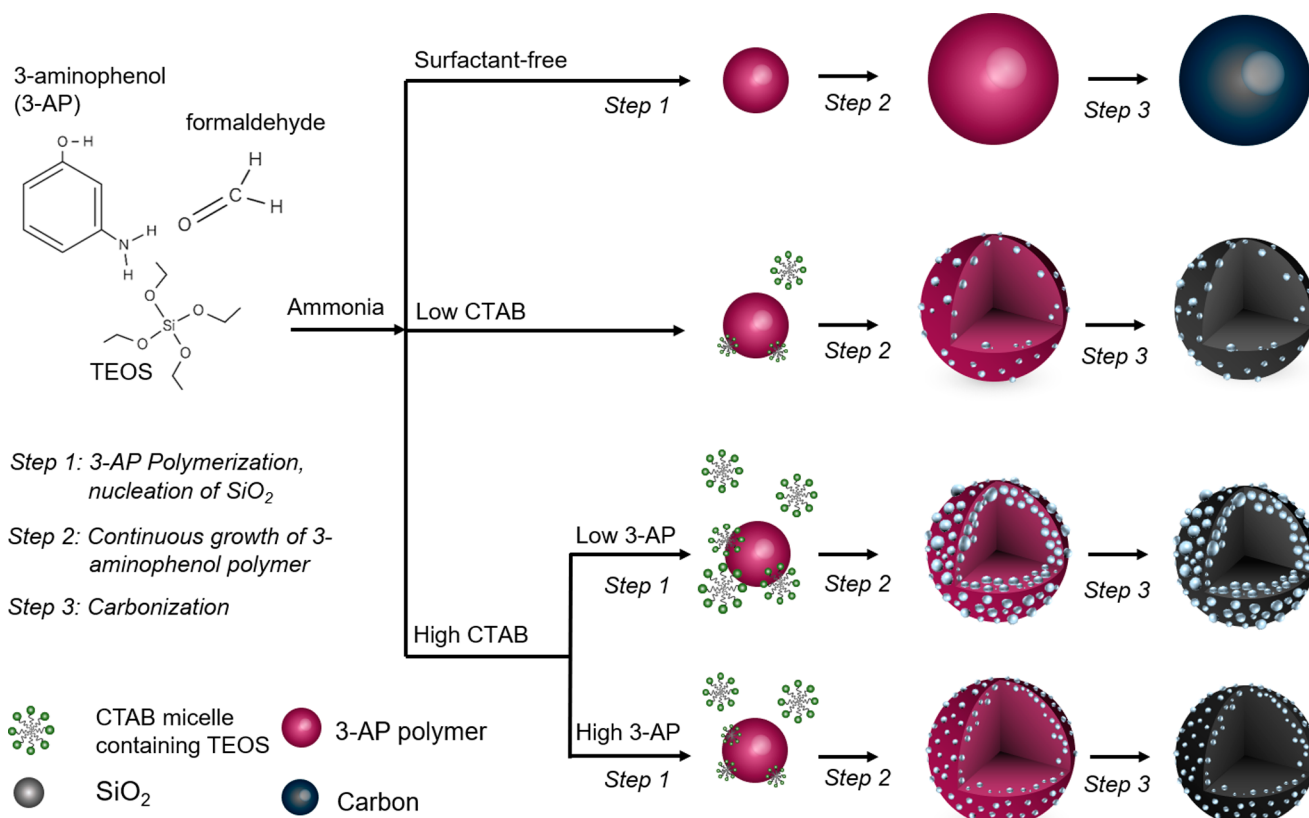


**Figure 6.** Summary of composite formation and effect of precursor composition on composite morphology.

nanoparticles on the surface and inside the composite. Carbon was removed from the composite structure and the effect of TEOS concentration on the SiO<sub>2</sub> structure was studied to facilitate observation of SiO<sub>2</sub> nanoparticle dispersion. Carbon was removed by calcination at the temperature at which sintering was estimated to be minimum. Minimum sintering was expected to prevent SiO<sub>2</sub> movement out of the initial structure on carbon removal. The results are shown in Figure 5. Figure 4b,c suggests that the SiO<sub>2</sub> nanoparticles were well dispersed on the surface. However, hardly any nanoparticles were present inside the composite as Figure 5 shows hollow SiO<sub>2</sub> particles with porous shells. The interior of the shell is shown by red dashed lines in Figure 5d–f. The formation of hollow SiO<sub>2</sub> particles implies that the core of the composite consisted mainly of carbon. This supports the proposed composite formation mechanism in which 3-aminophenol was polymerized prior to attracting SiO<sub>2</sub> seeds confined in the CTAB micelles, as shown in Figure 1.

The SEM and TEM images in Figure 5 also show that the SiO<sub>2</sub> nanoparticles served as the shell, which thickened with increasing TEOS concentration, regardless of the concentration of TEOS used in the synthesis. Shell thickening led to a denser shell structure. The morphology of the calcined composite suggests that this route is also promising for the synthesis of hollow SiO<sub>2</sub> particles with mesoporous shells. The composite formation mechanism is summarized in Figure 6 on the basis of the effects of the CTAB and 3-aminophenol concentrations.

X-ray photoelectron spectroscopy (XPS) was performed to identify the composite constituents. The C/SiO<sub>2</sub> composite synthesized using a 3-aminophenol concentration of 24 μM was used as an example. Figure 7a shows the core level Si 2p XP spectrum. Gaussian fitting shows a peak centroid at a binding

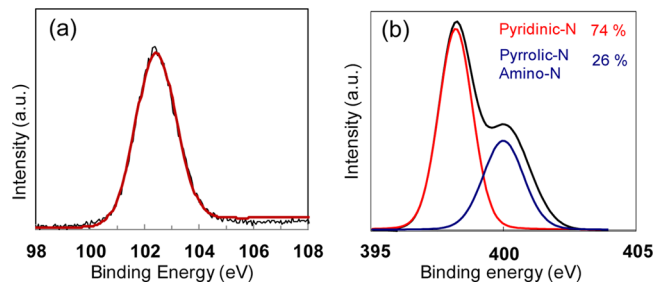


**Figure 7.** XP spectra: (a) Si 2p, which shows binding energy of 102.35 eV, and (b) N 1s, with contents of nitrogen functional groups.

energy of 102.35 eV. The binding energy for SiO<sub>2</sub> is 103.8 eV, but the observed value is closer to the binding energy for a siloxane, i.e., ≡Si–O–Si≡ (102.30 eV) or to those for silicon oxides with O/Si atoms less than 2, e.g., SiO<sub>1.24</sub> (102.4 eV).<sup>27</sup> However, the formation of substoichiometric silicon oxide is improbable because heating was performed in a mild environment in which reduction of SiO<sub>2</sub> was unlikely.<sup>28,29</sup> This suggests that the observed binding energy can probably be assigned to siloxane, which is an intermediate in TEOS hydrolysis and condensation.<sup>30</sup> This implies that the SiO<sub>2</sub> synthesized using this synthesis protocol is noncrystalline and contains traces of intermediates.

Previous research has shown the possibility of preserving the nitrogen atom of 3-aminophenol during polymerization and carbonization to give nitrogen-doped carbon structures. The elemental analysis results in Table 1 show that the nitrogen content in the composite was 5.34% after carbonization. The N 1s XP spectra in Figure 7b show that the carbon constituent contained 74% pyridinic nitrogen and 26% pyrrolic or amino

**Table 1. Elemental Analysis of Composite before and after Carbonization**

sample	elemental content (atom %)			
	C	N	O	Si
before carbonization	69.4	6.76	18.6	5.31
after carbonization	67.4	5.34	19.2	8.00

nitrogen. This characteristic is particularly beneficial for electrochemical applications, which take advantage of the free electrons in nitrogen functional groups. It is important to note that the elemental analysis results in Table 1 cannot be used to determine the O/Si atomic ratio because some of the O atoms are present in amorphous carbon.

The carbon constituent not only served as an anchor for nitrogen functional groups but also provided a porous structure. The pores in the carbon are mainly formed from gas released during precursor decomposition.<sup>4</sup> The presence of pores is confirmed by the nitrogen adsorption–desorption isotherm, which shows a combination of monolayer–multilayer adsorption in the presence of micropores (Figure 8a); the  $S_{\text{BET}}$  is 375  $\text{m}^2/\text{g}$ . Barrett–Joyner–Halenda analysis of the results (Figure 8b) shows a dominant pore size of 1.22 nm, with a total pore volume of 0.18  $\text{cm}^3/\text{g}$ .

### 3. EXPERIMENTAL SECTION

**3.1. Composite Synthesis.** All chemicals used in this work were analytical grade and used as received without further purification. Typically, an aqueous solution was prepared by stirring 3-aminophenol (Sigma-Aldrich, St. Louis, MO), ammonia solution (Kanto Chemical Co., Inc., Tokyo, Japan), and ultrapure water at room temperature until a clear solution was obtained. Cetyltrimethylammonium bromide (CTAB, Sigma-Aldrich, St. Louis, MO) dissolved in ethanol was added to the solution and the mixture was stirred for 15 min. TEOS (99.9%, Sigma-Aldrich, St. Louis, MO) and formaldehyde (Kanto Chemical Co., Inc., Tokyo, Japan) were simultaneously added to the solution. The mixture was subjected to microwave irradiation ( $\mu$ -Reactor, Shikokukeisokogyo, Kagawa, Japan) with the temperature being set at 40 °C. After 15 min, the temperature was elevated to 80 °C and kept constant for 60 min. The obtained particles were separated from the solution by centrifugation and washed several times with ultrapure water and ethanol to remove the remaining impurities. After drying, the particles were carbonized by heat

treatment in a nitrogen atmosphere (0.5 L/min) for 3 h at 550 °C. Details of the conditions for sample preparation are summarized in Table S1 in the Supporting Information.

**3.2. Physical Characterization.** The morphologies of the synthesized C/SiO<sub>2</sub> composites were examined using field-emission scanning electron microscopy (S-5000, 20 kV, Hitachi High-Tech. Corp., Tokyo, Japan) and transmission electron microscopy (TEM; JEM-2010, 200 kV, JEOL Ltd., Tokyo, Japan). The  $\zeta$ -potential and micelle size were determined by DLS (Zetasizer Nano ZSP, Malvern Instruments Ltd., Malvern, U.K.). Elemental analysis was performed using X-ray photoelectron spectroscopy (XPS; PHI Quantera II, Physical Electronics, Chanhassen, MN). The thermal behaviors before and after calcination were investigated using thermogravimetric analysis (TGA-50/51 Shimadzu Corp., Kyoto, Japan). The nitrogen adsorption–desorption properties of the C/SiO<sub>2</sub> composites were investigated with gas adsorption measurement equipment (BELSORP-max, MicrotracBEL Corp., Osaka, Japan), and the surface area was calculated by the Brunauer–Emmett–Teller (BET) method from the nitrogen isotherm curve.

### 4. CONCLUSIONS

A protocol for the rapid synthesis of C/SiO<sub>2</sub> composites was developed. The use of raw materials, i.e., TEOS and 3-aminophenol instead of presynthesized materials enabled better control of the SiO<sub>2</sub> nanoparticle morphology. This opens up a wide range of future applications. In this synthesis protocol, the cationic surfactant CTAB plays an important role, not only in composite formation but also in the hydrolysis and condensation of TEOS. Polymerization of 3-aminophenol and hydrolysis and condensation of TEOS were performed simultaneously, assisted by microwave irradiation to accelerate the reaction. Nitrogen doping is an additional feature of this method and is beneficial for applications involving electron transfer.

### ■ ASSOCIATED CONTENT

#### Supporting Information

The Supporting Information is available free of charge on the ACS Publications website at DOI: 10.1021/acsomega.8b00340.

List of samples and their experimental conditions, digital photograph of the SiO<sub>2</sub> synthesis in the absence of CTAB, DLS analysis (PDF)

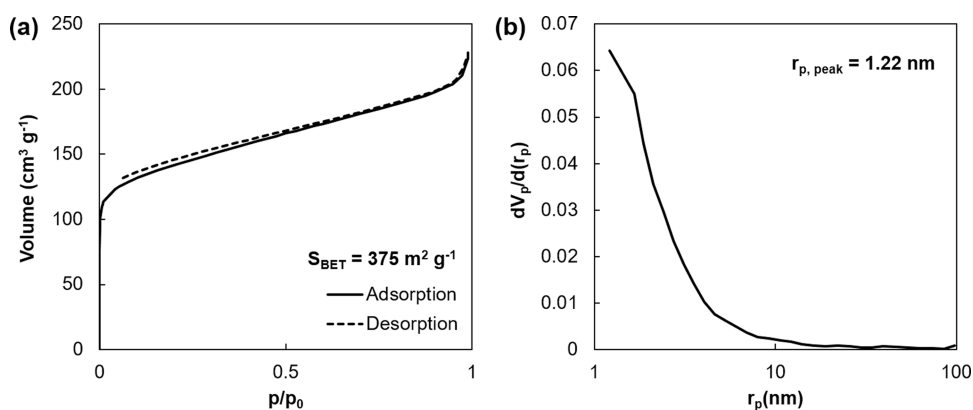


**Figure 8.** (a) Nitrogen adsorption–desorption isotherm and (b) pore size distribution based on Barrett–Joyner–Halenda analysis. C/SiO<sub>2</sub> composite synthesized using 24  $\mu\text{M}$  3-aminophenol was used as an example.

## AUTHOR INFORMATION

## Corresponding Author

\*E-mail: [ogit@hiroshima-u.ac.jp](mailto:ogit@hiroshima-u.ac.jp). Tel/Fax: +81-82-424-3765.

## ORCID

Aditya F. Arif: 0000-0003-4219-4395

Takashi Ogi: 0000-0003-3982-857X

## Notes

The authors declare no competing financial interest.

## ACKNOWLEDGMENTS

This work was supported by JSPS KAKENHI Grant Numbers 26709061 and 16K13642 and was partly supported by the Center for Functional Nano Oxides at Hiroshima University.

## REFERENCES

- (1) Yu, M.-F.; Lourie, O.; Dyer, M. J.; Moloni, K.; Kelly, T. F.; Ruoff, R. S. Strength and breaking mechanism of multiwalled carbon nanotubes under tensile load. *Science* **2000**, *287*, 637–640.
- (2) Wu, Z.-S.; Ren, W.; Gao, L.; Zhao, J.; Chen, Z.; Liu, B.; Tang, D.; Yu, B.; Jiang, C.; Cheng, H.-M. Synthesis of graphene sheets with high electrical conductivity and good thermal stability by hydrogen arc discharge exfoliation. *ACS Nano* **2009**, *3*, 411–417.
- (3) Arif, A. F.; Chikuchi, Y.; Balgis, R.; Ogi, T.; Okuyama, K. Synthesis of nitrogen-functionalized macroporous carbon particles via spray pyrolysis of melamine-resin. *RSC Adv.* **2016**, *6*, 83421–83428.
- (4) Arif, A. F.; Balgis, R.; Ogi, T.; Mori, T.; Okuyama, K. Experimental and theoretical approach to evaluation of nanostructured carbon particles derived from phenolic resin via spray pyrolysis. *Chem. Eng. J.* **2015**, *271*, 79–86.
- (5) Yu, D.; Goh, K.; Wang, H.; Wei, L.; Jiang, W.; Zhang, Q.; Dai, L.; Chen, Y. Scalable synthesis of hierarchically structured carbon nanotube-graphene fibres for capacitive energy storage. *Nat. Nanotechnol.* **2014**, *9*, 555.
- (6) Ogi, T.; Nandiyanto, A. B. D.; Okuyama, K. Nanostructuring strategies in functional fine-particle synthesis towards resource and energy saving applications. *Adv. Powder Technol.* **2014**, *25*, 3–17.
- (7) Abe, H.; Abe, I.; Sato, K.; Naito, M. Dry powder processing of fibrous fumed silica compacts for thermal insulation. *J. Am. Ceram. Soc.* **2005**, *88*, 1359–1361.
- (8) Yang, C. M.; Cho, A.-T.; Pan, F.-M.; Tsai, T.; Chao, K. Spin-on Mesoporous Silica Films with Ultralow Dielectric Constants, Ordered Pore Structures, and Hydrophobic Surfaces. *Adv. Mater.* **2001**, *13*, 1099–1102.
- (9) Fang, Y.; Zheng, G.; Yang, J.; Tang, H.; Zhang, Y.; Kong, B.; Lv, Y.; Xu, C.; Asiri, A. M.; Zi, J.; et al. Dual-Pore Mesoporous Carbon@Silica Composite Core-Shell Nanospheres for Multidrug Delivery. *Angew. Chem.* **2014**, *126*, 5470–5474.
- (10) Xue, C.; Tu, B.; Zhao, D. Evaporation-Induced Coating and Self-Assembly of Ordered Mesoporous Carbon-Silica Composite Monoliths with Macroporous Architecture on Polyurethane Foams. *Adv. Funct. Mater.* **2008**, *18*, 3914–3921.
- (11) Yang, X.; Huang, H.; Li, Z.; Zhong, M.; Zhang, G.; Wu, D. Preparation and lithium-storage performance of carbon/silica composite with a unique porous bicontinuous nanostructure. *Carbon* **2014**, *77*, 275–280.
- (12) Li, M.; Yu, Y.; Li, J.; Chen, B.; Wu, X.; Tian, Y.; Chen, P. Nanosilica/carbon composite spheres as anodes in Li-ion batteries with excellent cycle stability. *J. Mater. Chem. A* **2015**, *3*, 1476–1482.
- (13) Cao, M.-S.; Song, W.-L.; Hou, Z.-L.; Wen, B.; Yuan, J. The effects of temperature and frequency on the dielectric properties, electromagnetic interference shielding and microwave-absorption of short carbon fiber/silica composites. *Carbon* **2010**, *48*, 788–796.
- (14) Pol, V. G.; Pol, S.; George, P.; Markovsky, B.; Gedanken, A. Synthesis of a Conducting SiO<sub>2</sub>-Carbon Composite from Commercial Silicone Grease and Its Conversion to Paramagnetic SiO<sub>2</sub> Particles. *J. Phys. Chem. B* **2006**, *110*, 13420–13424.
- (15) Kim, J.-H.; Sohn, H.-J.; Kim, H.; Jeong, G.; Choi, W. Enhanced cycle performance of SiO-C composite anode for lithium-ion batteries. *J. Power Sources* **2007**, *170*, 456–459.
- (16) Zhang, J.; Zhang, C.; Liu, Z.; Zheng, J.; Zuo, Y.; Xue, C.; Li, C.; Cheng, B. High-performance ball-milled SiO<sub>x</sub> anodes for lithium ion batteries. *J. Power Sources* **2017**, *339*, 86–92.
- (17) Yao, Y.; Zhang, J.; Xue, L.; Huang, T.; Yu, A. Carbon-coated SiO<sub>2</sub> nanoparticles as anode material for lithium ion batteries. *J. Power Sources* **2011**, *196*, 10240–10243.
- (18) Zhao, J.; Luque, R.; Qi, W.; Lai, J.; Gao, W.; Gilani, M. R. H. S.; Xu, G. Facile surfactant-free synthesis and characterization of Fe<sub>3</sub>O<sub>4</sub>@3-aminophenol-formaldehyde core-shell magnetic microspheres. *J. Mater. Chem. A* **2015**, *3*, 519–524.
- (19) Zhao, J.; Niu, W.; Zhang, L.; Cai, H.; Han, M.; Yuan, Y.; Majeed, S.; Anjum, S.; Xu, G. A template-free and surfactant-free method for high-yield synthesis of highly monodisperse 3-aminophenol-formaldehyde resin and carbon nano/microspheres. *Macromolecules* **2013**, *46*, 140–145.
- (20) Balgis, R.; Arif, A. F.; Mori, T.; Ogi, T.; Okuyama, K.; Anilkumar, G. M. Morphology-dependent electrocatalytic activity of nanostructured Pt/C particles from hybrid aerosol-colloid process. *AIChE J.* **2016**, *62*, 440–450.
- (21) Arif, A. F.; Kobayashi, Y.; Schneider, E. M.; Hess, S. C.; Balgis, R.; Izawa, T.; Iwasaki, H.; Taniguchi, S.; Ogi, T.; Okuyama, K.; Stark, W. J. Selective Low-energy Carbon Dioxide Adsorption using Monodisperse Nitrogen-rich Hollow Carbon Submicron Spheres. *Langmuir* **2017**, *34*, 30–35.
- (22) Arif, A. F.; Kobayashi, Y.; Balgis, R.; Ogi, T.; Iwasaki, H.; Okuyama, K. Rapid microwave-assisted synthesis of nitrogen-functionalized hollow carbon spheres with high monodispersity. *Carbon* **2016**, *107*, 11–19.
- (23) Dhara, D.; Shah, D. O. Effect of poly (ethylene glycol) s on micellar stability of sodium dodecyl sulfate. *Langmuir* **2001**, *17*, 7233–7236.
- (24) Siddiquey, I. A.; Furusawa, T.; Sato, M.; Suzuki, N. Microwave-assisted silica coating and photocatalytic activities of ZnO nanoparticles. *Mater. Res. Bull.* **2008**, *43*, 3416–3424.
- (25) Li, W.; Han, Y.-C.; Zhang, J.-L.; Wang, L.-X.; Song, J. Thermodynamic modeling of CTAB aggregation in water-ethanol mixed solvents. *Colloid J.* **2006**, *68*, 304–310.
- (26) Cates, M.; Candau, S. Statics and dynamics of worm-like surfactant micelles. *J. Phys.: Condens. Matter* **1990**, *2*, 6869.
- (27) Alfonsetti, R.; Lozzi, L.; Passacantando, M.; Picozzi, P.; Santucci, S. XPS studies on SiO<sub>x</sub> thin films. *Appl. Surf. Sci.* **1993**, *70–71*, 222–225.
- (28) Cui, J.; Cui, Y.; Li, S.; Sun, H.; Wen, Z.; Sun, J. Microsized Porous SiO<sub>x</sub>@C Composites Synthesized through Aluminothermic Reduction from Rice Husks and Used as Anode for Lithium-Ion Batteries. *ACS Appl. Mater. Interfaces* **2016**, *8*, 30239–30247.
- (29) Shi, L.; Wang, W.; Wang, A.; Yuan, K.; Jin, Z.; Yang, Y. Scalable synthesis of core-shell structured SiO<sub>x</sub>/nitrogen-doped carbon composite as a high-performance anode material for lithium-ion batteries. *J. Power Sources* **2016**, *318*, 184–191.
- (30) Chen, S.-L.; Dong, P.; Yang, G.-H.; Yang, J.-J. Kinetics of formation of monodisperse colloidal silica particles through the hydrolysis and condensation of tetraethylorthosilicate. *Ind. Eng. Chem. Res.* **1996**, *35*, 4487–4493.